Generalized random matrix model with additional interactions

Swapnil Yadav, Kazi Alam and K. A. Muttalib

Department of Physics, University of Florida, Gainesville, FL 32611-8440, USA

E-mail: yadavswap.12@ufl.edu, kazi.a.alam@ufl.edu and muttalib@phys.ufl.edu

Dong Wang

Department of Mathematics, National University of Singapore, Singapore

E-mail: matwd@nus.edu.sg

Abstract. We introduce a generalized form of the random matrix ensemble with additional interaction, the strength of which depends on a parameter γ. The equilibrium density is computed by numerically solving the Riemann-Hilbert problem associated with the ensemble. The effect of the additional parameter γ associated with the two-body interaction can be understood in terms of an effective γ-dependent single-particle confining potential.

13 August 2019

1. Introduction

The Wigner-Dyson random matrix ensembles (see e. g. [1]) introduced to explain the nuclear energy-level fluctuations are characterized by the joint probability distribution (jpd) of the eigenvalues

$$p(\{x_i\}) \propto \prod_{i=1}^{N} w(x_i) \prod_{i<j} |x_i - x_j|^{\beta}, \quad w(x) = e^{-V(x)} \text{ or } w(x) = e^{-NV(x)} \tag{1}$$

where $\beta = 2$ for unitary ensembles. Throughout this paper, we assume the convention $w(x) = e^{-NV(x)}$, so that the empirical distribution of the particles (aka equilibrium measure) converges as $N \to \infty$. It is useful to describe the jpd in terms of an effective 'Hamiltonian' H of the eigenvalues defined by $p = \exp(-\beta H)$, where the term $\ln |x_i - x_j|$ in H corresponds to a "two-body interaction", while the term $\frac{1}{\beta} V(x)$ corresponds to a single particle "confining potential".

As a toy model for quasi one-dimensional (1D) disordered conductors [2], a solvable random matrix model with an additional two-body interaction was proposed in [3],

$$p(\{x_i\}; \theta) \propto \prod_{i=1}^{N} w(x_i) \prod_{i<j} |x_i - x_j||x_i^{\theta} - x_j^{\theta}|. \tag{2}$$

This model was studied in detail by Borodin [4], and has become known as the Muttalib-Borodin (MB) ensemble [5], [6], [7]. The special case of $\theta = 2$ was later considered in [8] as a model of disordered bosons.

It has later been argued that in contrast to a quasi 1D system, describing a three-dimensional (3D) disordered conductor with appropriate eigenvector correlations needs a disorder-dependent parameter γ that controls the strength of the two-body interaction [9], [10], [11], [12]. The generic form that captures the essential features of this quasi 1D to 3D generalization has been suggested to be of the form

$$p(\{x_i\}; \gamma) \propto \prod_{i=1}^{N} w(x_i) \prod_{i<j} |x_i - x_j||r(x_i) - r(x_j)|^{\gamma}, \quad 0 < \gamma \leq 1, \tag{3}$$

where $r(x)$ and $w(x)$ are appropriate functions relevant for disordered conductors [12]. As a solvable toy model that allows us to explore and study the role of the parameter γ, we propose to investigate the simplest generalization of the MB ensemble, with $r(x) = x^{\theta}$ and $V(x) = 2x$:

$$p(\{x_i\}; \theta, \gamma) \propto \prod_{i=1}^{N} w(x_i) \prod_{i<j} |x_i - x_j||x_i^{\theta} - x_j^{\theta}|^{\gamma}, \quad 0 < \gamma \leq 1. \tag{4}$$

In particular, we will consider the case $\theta = 2$ in detail, although the method is applicable for any $\theta > 1$ and for any well behaved external confining potential. We will be interested in the case $x_i \geq 0$, since the transmission eigenvalues are non-negative [13]. We will call it the γ-ensemble. Note that $\gamma = 1$ is just the MB ensemble of Eq. (2).

By solving the associated Riemann-Hilbert (RH) problem [14], Claeys and Romano, henceforth referred to as CR [15], have obtained the density of eigenvalues for the MB ensembles (Eq. (2)) for a linear as well as a quadratic potential, which have power-law divergences at the hard edge for all $\theta > 1$. In this work we generalize the method developed by CR to the case of the γ-ensemble (Eq. (4)) and study the density as a function of γ. Our results suggest that the γ-ensemble can be mapped on to an MB ensemble by replacing the single particle confining potential $V(x)$ with a γ-dependent effective potential $V_{\text{eff}}(x;\gamma)$. This allows us to calculate the density for arbitrary values of γ. In particular we will show that as γ is systematically reduced from 1, the exponent of the diverging density at the hard edge changes from $-1/3$ for $\gamma = 1$ (the MB ensemble) to $-1/2$ for $\gamma = 0$ (the orthogonal Laguerre ensemble).

For the sake of completeness, we will repeat the method to study the effect of γ on a model with non-diverging density, that is, with no hard edge. In particular we will apply the method to consider a model with a different two-body interaction, $r(x) = e^x$ with $-\infty < x < +\infty$, where the corresponding density has two soft edges. This shows that as long as the Joukowsky Transformation(JT) is known, the method can be applied to a wide variety of generalized models.

The paper is organized as follows. In Section 2 we briefly outline the equilibrium problem and the JT following CR. In Sections 3 and 4 we show how the method of CR can be adapted for the γ-ensembles to obtain the effective potential and the level density. In Section 5 we use $V(x) = 2x$ to show how the effective potentials and the corresponding level-densities change as γ is reduced from 1 towards zero. Finally in Section 6 we show briefly how the method can be applied to the case of $r(x) = e^x$ and $V(x) = \frac{x^2}{2}$ for which the JT was obtained by Claeys and Wang [16], henceforth referred to as CW, and the density is non-diverging. Details of this model are provided in the Appendix.

2. The equilibrium problem

In terms of the Hamiltonian in (4), by potential theory, there exists a unique equilibrium measure that minimizes the corresponding energy functional which satisfies the Euler-Lagrange (EL) equation

$$\int \ln|x_i - x_j| d\mu(x_i) + \gamma \int \ln|x_i^\theta - x_j^\theta| d\mu(x_i) - V(x_j) = \ell \tag{5}$$

if x_j lies inside the support of density. Here ℓ is some constant. Also the empirical distribution of the particles with Hamiltonian (4) converges to this equilibrium measure. The equality sign is replaced by $<$ if x lies outside the support. The equilibrium problem for $\gamma = 1$ has been solved exactly in CR.‡ In solving for the corresponding density, a

‡ To be precise, CR solves the equilibrium problem under the "one-cut" condition that requires the equilibrium measure to be supported on a single interval. All the potentials, including the effective

crucial role is played by the Joukowsky Transformation (JT)

$$\begin{aligned} J_c(s) &= c(s+1)(\frac{s+1}{s})^{\frac{1}{\theta}}, \quad \text{for hard edge} \\ J_{c_1,c_0}(s) &= (c_1 s + c_0)(\frac{s+1}{s})^{\frac{1}{\theta}}, \quad \text{for soft edge} \end{aligned} \tag{6}$$

where s is a complex variable. The hard edge corresponds to a support interval $[0, b]$, $b > 0$ being a real number, while support for soft edge is $[a, b]$ where both a and b are real numbers with $a < b$. From the JT associated with a given jpd, equilibrium density can be obtained by solving the vector-valued RH problem. While the JT in (6) was obtained for $\gamma = 1$, it turns out that the equilibrium problem for $\gamma < 1$ can also be solved with the same transformations. In the following two sections we will briefly outline how the above JT can be used to obtain the density for arbitrary $0 < \gamma < 1$.

3. Effective potential

To accommodate $0 < \gamma < 1$ for non-negative eigenvalues within the CR framework, we consider the hard edge case, focusing on $\theta = 2$ for simplicity.

The JT for hard edge is analytic in $\mathbb{C}\backslash[-1, 0]$ and has critical points on real line at $S_a = -1$ and $S_b = \frac{1}{\theta}$ which are mapped to points 0 and $b = c\frac{(1+\theta)^{1+\frac{1}{\theta}}}{\theta}$, respectively. There also exist points in the complex plane which are mapped on to the real line between 0 and b by $J_c(s)$. The equation of locus of such points is given by

$$r(\phi) = \tan\left(\frac{\phi}{1+\theta}\right) \Big/ \left[\sin\phi - \cos\phi \tan\left(\frac{\phi}{1+\theta}\right)\right], \tag{7}$$

where $0 < \phi < 2\pi$ is the argument of point s in the complex plane. This defines a closed contour ν in the complex plane which is symmetric about the x-axis. We denote the two symmetric parts as curves ν_1 (upper) and ν_2 (lower) which are complex conjugates of each other. Figure 1 and Figure 2 show contour ν for $\theta = 2, c = 1$ and its mapping, respectively. Since this mapping calculation is numerical, in Figure 2 we see very small y components as well. In this paper we orient ν positively, so ν_1 is from right to left and and ν_2 is from left to right. In Figure 3 we show details of this mapping schematically. In particular, all points except the branch cut $[-1, 0]$ in the region D inside the contour ν is mapped on to a complex region $\mathbb{H}_\theta\backslash[0, b]$, while all outside points are mapped on to a different complex region $\mathbb{C}\backslash[0, b]$.

To solve for $\mu(x)$ using the EL equations we define complex transforms in two regions as follows,

$$\begin{aligned} g(z) &\equiv \int_0^b \log(z - x) d\mu(x), \quad z \in \mathbb{C}\backslash(-\infty, b]; \\ \tilde{g}(z) &\equiv \int_0^b \log(z^\theta - x^\theta) d\mu(x), \quad z \in \mathbb{H}_\theta\backslash(0, b]. \end{aligned} \tag{8}$$

potentials, satisfy this condition, so we do not give an extensive discussion to it.

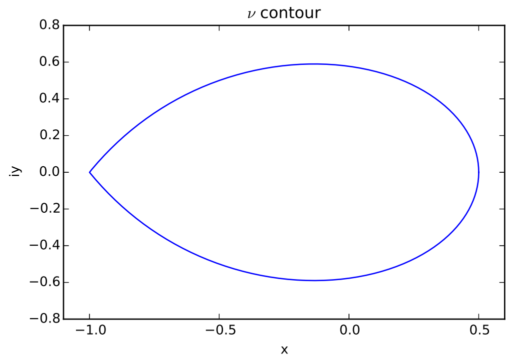

Figure 1. (Color online) ν contour for $\theta = 2,\ c = 1$.

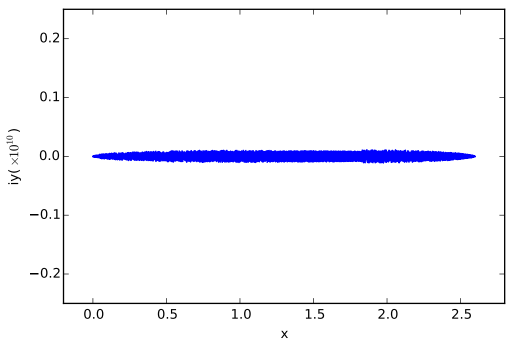

Figure 2. (Color online) Mapping for ν_1 contour, $\theta = 2,\ c = 1$. Mapping for ν_2 looks similar.

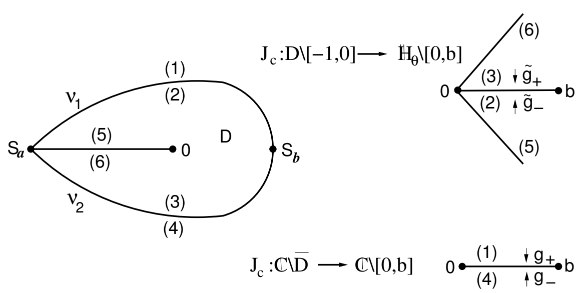

Figure 3. (Color online) Schematic Figure for mapping of JT, following CR.

Here $(g, \tilde{g})$ is analytic in $(\mathbb{C}\backslash(-\infty, b], \mathbb{H}_\theta\backslash(0, b])$ respectively so that the logarithms are well defined. Let g_+, g_- and $\tilde{g}_+, \tilde{g}_-$ denote boundary values of g and $\tilde{g}$ when approaching $(-\infty, b]$ in $\mathbb{C}$ and $(0, b]$ in $\mathbb{H}_\theta$ respectively from above $(+)$ and below $(-)$, as shown schematically in Figure 3. We have for $x \in [0, b]$

$$g_\pm(x) = \int_0^b \ln|x - y| d\mu(y) \pm \pi i \mu([x, b]), \quad \tilde{g}_\pm(x) = \int_0^b \ln|x^\theta - y^\theta| d\mu(y) \pm \pi i \mu([x, b]). \tag{9}$$

From EL equations we can write

$$g_{\pm}(x) + \gamma \tilde{g}_{\mp}(x) - V(x) - \ell = \pm \pi i (1-\gamma)\mu([x,b]). \tag{10}$$

Rewriting $g = (1+\gamma)g/2 + (1-\gamma)g/2$ the two EL equations become

$$\left(\frac{1 \pm \gamma}{2}\right) g_{+}(x) + \left(\frac{1 \mp \gamma}{2}\right) g_{-}(x) + \gamma \tilde{g}_{\mp}(x) = V(x) + \ell. \tag{11}$$

Following CR, we define $G(s) \equiv g'(s)$ and $\tilde{G}(s) \equiv \tilde{g}'(s)$ where the prime denotes derivative with respect to its argument. Also define

$$M(s) \equiv \begin{cases} G(J_c(s)), & \text{for } s \in \mathbb{C}\backslash\bar{D}, \\ \tilde{G}(J_c(s)), & \text{for } s \in D\backslash[-1,0], \end{cases} \tag{12}$$

where D is the domain inside ν, as shown in Figure 3. For $x \in (0,b)$, there are $s_1 \in \nu_1$ and $s_2 \in \nu_2$ such that $J_c(s_1) = J_c(s_2) = x$. Then for $g_+(x)$ in Eq. (11), it is equal to the limit of $g(J_c(s))$ as $s \to s_1 \in \nu_1$ from outside of contour ν (see Figure 3). Similarly for $\tilde{g}_+(x)$, it is equal to the limit of $\tilde{g}(J_c(s))$ as $s \to s_2 \in \nu_2$ from inside of contour ν. Hence by taking derivative, the properties of $g_{\pm}(x)$ above implies the properties of $M(s)$

$$\begin{aligned} M_+(s_1) + \gamma M_-(s_1) + M_-(s_2) + \gamma M_+(s_2) &= 2V'(J_c(s)), \\ M_+(s_1) - M_-(s_2) + M_-(s_1) - M_+(s_2) &= 0. \end{aligned} \tag{13}$$

Following CR we define $N(s) \equiv M(s)J_c(s)$, so (13) can be rewritten in terms of $N(s)$ and $J_c(s)$. In addition, $J_c(s_1^+) = J_c(s_1^-) = x$ where $J_c(s_1^+)$ (resp. $J_c(s_1^-)$) is the limit of $J_c(s)$ with s approaching $s_1 \in \nu_1$ from outside (resp. inside) of ν(see Figure 3). Thus we can replace both $J_c(s_1^+)$ and $J_c(s_1^-)$ by $J_c(s) = x$. We have

$$\begin{aligned} N_+(s_1) + \gamma N_-(s_1) + N_-(s_2) + \gamma N_+(s_2) &= 2V'(J_c(s))J_c(s), \\ N_+(s_1) - N_-(s_2) + N_-(s_1) - N_+(s_2) &= 0. \end{aligned} \tag{14}$$

We further define a function f such that

$$f(J_c(s)) \equiv N_+(s) + N_-(s), \tag{15}$$

with solution to $N(s)$ as,

$$N(s) = \begin{cases} \frac{-1}{2\pi i}\oint_\nu \frac{f(J_c(\xi))}{\xi - s}\, d\xi + 1, & s \in \mathbb{C}\backslash\bar{D}, \\ \frac{1}{2\pi i}\oint_\nu \frac{f(J_c(\xi))}{\xi - s}\, d\xi - 1, & s \in D\backslash[-1,0] \end{cases} \tag{16}$$

where contour ν is for JT $J_c(s)$ [15]. The constant c in this JT satisfies the equation

$$\frac{1}{2\pi i}\oint_\nu \frac{f(J_c(s))}{s} ds = 1 + \theta. \tag{17}$$

Equation (14) can now be rewritten as

$$(1-\gamma)(N_+(s_1) + N_-(s_2)) + 2\gamma f(J_c(s)) = 2V'(J_c(s))J_c(s). \tag{18}$$

From Equation(16) we have,

$$N_+(s_1) = \frac{1}{2\pi i}\oint_\nu \frac{f(J_c(s))}{(s_1)_+ - s}ds + 1, \quad N_-(s_2) = \frac{1}{2\pi i}\oint_\nu \frac{f(J_c(s))}{(s_2)_- - s}ds + 1. \tag{19}$$

Let us now define the inverse mapping of J_c as

$$s = J_c^{-1}(x) = h(x). \tag{20}$$

It is generally double-valued, and we can take the appropriate one. Note that for both $N_+(s_1)$ and $N_-(s_2)$ in Eq. (19), the function is defined by the limit of $N(s)$ as s approaches s_1 or s_2 on ν from outside. Hence we used the first identity in Eq. (16). Let $(s_1)_+ = h(y)$; $(s_2)_- = \bar{h}(y)$; $s_1 = h(x)$ and $s_2 = \bar{h}(x)$ where the bar denotes complex conjugate. ($h(y) - h(x)$ is infinitesimal if $y = x$, but it is crucial that $h(y)$ is outside of γ while $h(x)$ is on γ.) Writing Eq. (19) in terms of the inverse mappings we get

$$\begin{aligned} N_+(s_1) &= \frac{1}{2\pi i}\int_{\nu_1} \frac{f(x)}{h(y) - h(x)}dh(x) + \frac{1}{2\pi i}\int_{\nu_2} \frac{f(x)}{h(y) - \bar{h}(x)}d\bar{h}(x) + 1, \\ N_-(s_2) &= \frac{1}{2\pi i}\int_{\nu_1} \frac{f(x)}{\bar{h}(y) - h(x)}dh(x) + \frac{1}{2\pi i}\int_{\nu_2} \frac{f(x)}{\bar{h}(y) - \bar{h}(x)}d\bar{h}(x) + 1. \end{aligned} \tag{21}$$

Recall that ν_1 is oriented from S_b to S_a. Thus in the mapped space, limits of the corresponding real integral are from b to 0. Similarly for ν_2, the real integral is from 0 to b. Combining the two, writing the integrals in the mapped real space and substituting for $[N_+(s_1) + N_-(s_2)]$ we finally get the integral equation for f,

$$f(y;\gamma) = \frac{V'(y)y}{\gamma} - \frac{1-\gamma}{\gamma}\left[1 + \frac{1}{2\pi}\int_0^b f(x;\gamma)\phi(x,y)dx\right], \tag{22}$$

where

$$\phi(x,y) = \mathrm{Im}\left[\left(\frac{1}{h(y) - \bar{h}(x)} + \frac{1}{\bar{h}(y) - \bar{h}(x)}\right)\bar{h}'(x)\right]. \tag{23}$$

We solve the above integral equation (22) for $f(y;\gamma)$ and Eq. (17) for c numerically self-consistently. Using the definition for $f(x;\gamma)$ we further find the new effective potential $V_{\text{eff}}(x;\gamma)$ which is related to $f(x;\gamma)$ by

$$V'_{\text{eff}}(x;\gamma) = \frac{f(x;\gamma)}{x}. \tag{24}$$

This is one of the central results of this work. It shows that at the global density level the γ-ensembles can be mapped onto an MB ensemble with an appropriate effective single-particle potential. Thus methods developed for studying the MB ensemble can be adapted to study the γ-ensembles.

4. Level density

With given definition of V_{eff}, the constant c for JT satisfies equation similar to the one in CR except that V is now replaced by V_{eff}.

$$\frac{1}{2\pi i}\oint_{\nu}\frac{U_c(s)}{s}ds = 1+\theta, \quad U_c(s) = V'_{\text{eff}}(J_c(s);\gamma)J_c(s) = f(J_c(s);\gamma). \tag{25}$$

Then the density corresponding to the γ-ensembles is computed using the relation [15] $\sigma(y) = -[N_+(s_1) - N_-(s_2)]/2\pi iy$. Substituting for $N_+(s_1)$ and $N_-(s_2)$ using Eq. (16), the expression for density becomes,

$$\begin{aligned}\sigma(y;\gamma) &= \frac{-1}{2\pi^2\gamma y}\int_b^0 xV'_{\text{eff}}(x;\gamma)\chi(x,y)dx,\\ \chi(x,y) &= \text{Re}\left[\left(\frac{1}{\overline{h}(y)-h(x)} - \frac{1}{h(y)-h(x)}\right)h'(x)\right].\end{aligned} \tag{26}$$

The inverse mappings h and $\overline{h}$ are from complex mapping $[0,b]$ to the contour ν. Comparing with CR, it shows that the density for $\gamma < 1$ has the same expression as that for $\gamma = 1$, except that the potential $V(x)$ is replaced by the corresponding effective potential $V_{\text{eff}}(x;\gamma)$.

5. Results for $\theta = 2$

The formulation developed so far is independent of the choice of the confining potential $V(x)$. As a concrete example, we consider a potential of the form

$$V(x) = tx. \tag{27}$$

We will choose $t = 2$ as in CR. We consider the hard edge case for $\gamma < 1$ and $\theta = 2$. We solve the self-consistent integral equation (Eq. (22)) for $f(x;\gamma)$ numerically for different values of γ. Figure 4 shows $f(x;\gamma)$ for selected values of γ. Using the definition Eq. (24), we computed the corresponding $V_{\text{eff}}(x;\gamma)$ for each γ. Figure 5 shows the results.

The densities evaluated from the effective potentials for different γ are shown in Figure 6. The diverging exponent at the hard edge changes as a function of γ. Figure 7 shows the crossover between the known exponents -1/3 for $\gamma = 1$ and -1/2 for $\gamma = 0$ as a function of γ.

6. Non-diverging density

Finally, as an example of a model with non-diverging density which has two soft edges, we consider a γ-generalization of the model (3) with $r(x) = e^x$ and $w(x) = e^{\frac{-Nx^2}{2}}$, where $-\infty < x < +\infty$:

$$p(\{x_i\};\gamma) \propto \prod_{i=1}^{N} w(x_i)\prod_{i<j}|x_i - x_j||e^{x_i} - e^{x_j}|^{\gamma}, \quad 0 < \gamma \leq 1. \tag{28}$$

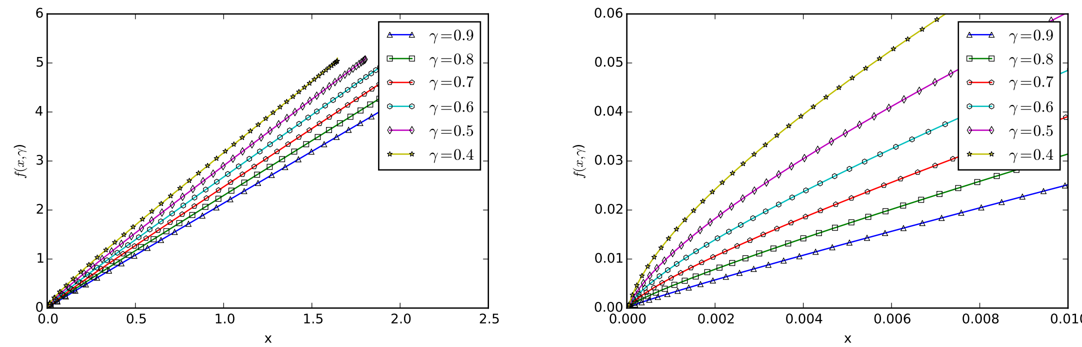

Figure 4. (Color online) Left panel: $f(x;\gamma)$ for different values of γ. Right panel: Expanded view near origin.

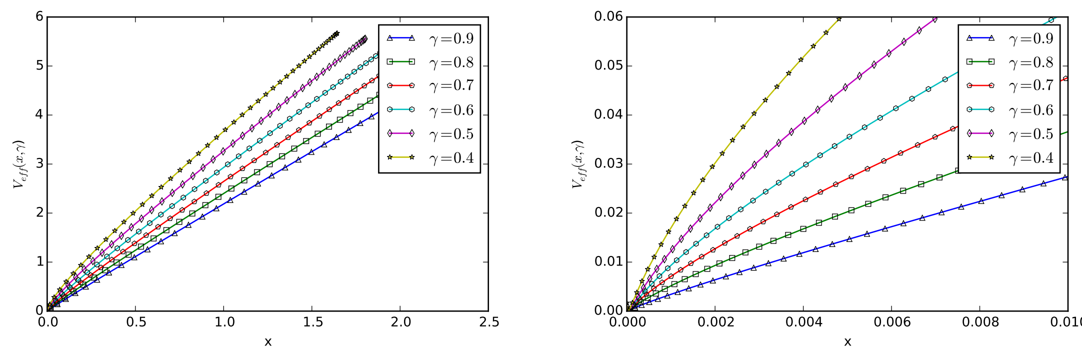

Figure 5. (Color online) Left panel: $V_{\mathrm{eff}}(x;\gamma)$ for different values of γ. Right panel: Expanded view near origin.

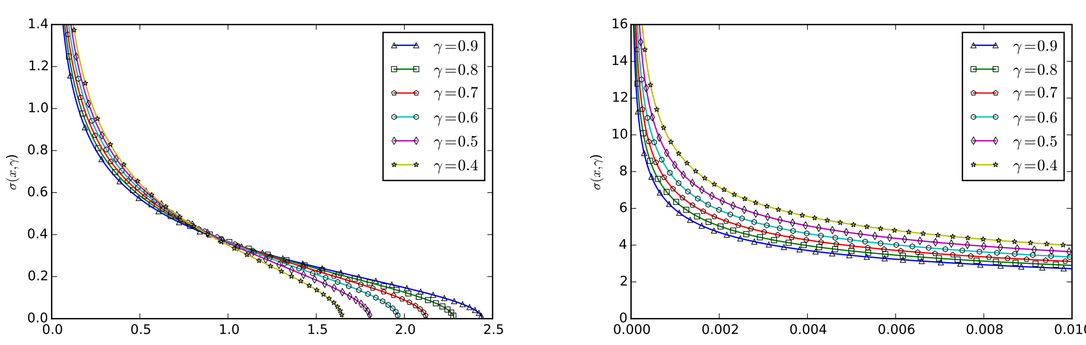

Figure 6. (Color online) Left panel: Normalized density corresponding to V_{eff} in Figure 5. Right panel: Expanded view near origin

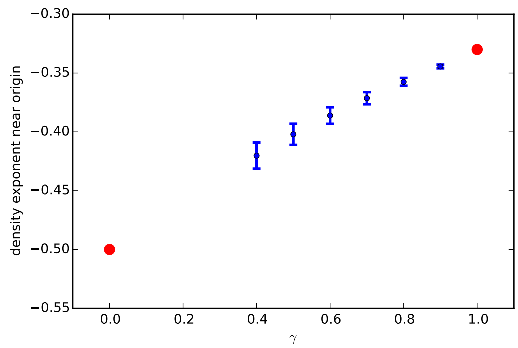

Figure 7. (Color online) Exponents with uncertainties in the numerical estimates. Points for $\gamma = 1$ and $\gamma = 0$ are known analytically.

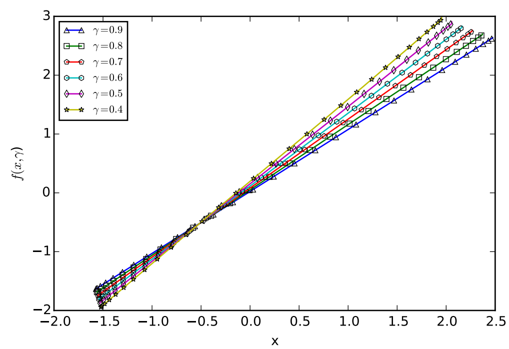

Figure 8. (Color online) $f_e(x;\gamma)$ for different values of γ.

The model with $\gamma = 1$ has been studied in detail by CW[16], who obtained the necessary JT. As with the generalized MB ensemble, we use the JT of CW and follow the method developed in Sections 3 and 4 to obtain the effective potential and hence the density for (28) for different values of γ. We present the details in the Appendix. The results for $f_e(x)$, the effective potentials and the densities for different values of γ are given in Figures 8 and 9.

7. Summary and conclusion

We have introduced a toy model, Eq. (4), as a generalization of the MB random matrix ensemble, Eq. (2), with an additional parameter γ. This model is a solvable version of a realistic model for 3D conductors, albeit with a simplified two-body interaction. In order to solve for the density, we develop a method based on the solution of the associated RH problem, following CR. In principle, any two-body interaction can be solved provided the appropriate JT is known. As an example, we also consider an interaction of the form $\ln |e^{x_i} - e^{x_j}|$ with $\infty < x < +\infty$ for which the JT has been obtained by CW. It would be interesting to consider this latter model with a hard edge, in order to be able

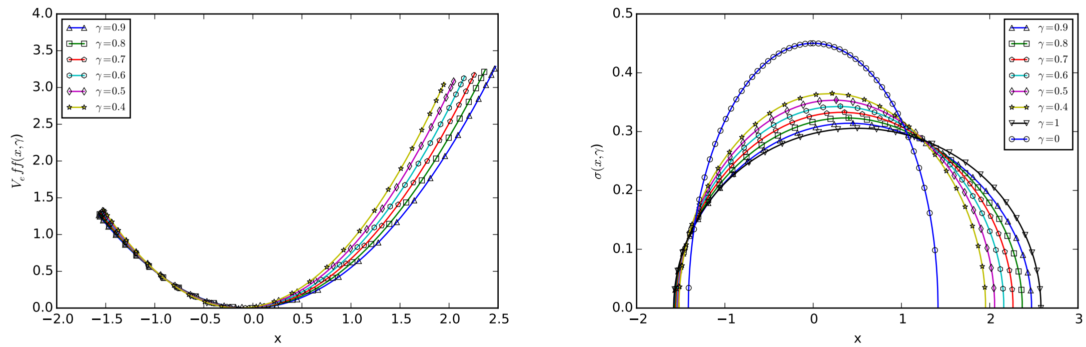

Figure 9. (Color online) The effective potential (Left panel) and the density (Right panel) for model (28). Densities for $\gamma = 1$ and $\gamma = 0$ are known analytically.

.

to compare how different two-body interactions affect the role of the parameter γ.

Our method exploits the fact that the effect of the parameter γ can be understood in terms of an effective γ-dependent potential $V_{\text{eff}}(x;\gamma)$, which replaces the starting confining potential $V(x)$. Hopefully, this will allow us to obtain not only the density, but also the two-level kernel from which correlations like the gap-function and the nearest-neighbor spacing distributions can be obtained.

Acknowledgments

KAM would like to thank the Department of Mathematics, NUS where he spent part of his sabbatical in 2017 and where this work originated. DW was partially supported by the Singapore AcRF Tier 1 grant R-146-000-217-112 (which partially supported KAM's visit) and the Chinese NSFC grant 11871425.

Appendix

Following CW, the JT for model (28) is

$$J_{c_1,c_0}(s) = c_1 s + c_0 - \log\frac{s-\frac{1}{2}}{s+\frac{1}{2}} \tag{29}$$

where s is a complex variable. Note that the transformation now contains two parameters c_0 and c_1 to include the two supports for the soft-edges given by $[a, b]$ where both a and b are real numbers such that $a < b$. The JT is analytic in $\mathbb{C}\backslash[-\frac{1}{2}, \frac{1}{2}]$ and has critical points on real line at $S_a = -\sqrt{\frac{1}{4}+\frac{1}{c_1}}$ and $S_b = \sqrt{\frac{1}{4}+\frac{1}{c_1}}$ which are mapped to points $a = J_{c_1,c_0}(S_a)$ and $b = J_{c_1,c_0}(S_b)$ respectively. There also exist points in the complex plane which are mapped to real line between a and b by $J_{c_1,c_0}(s)$. The equation

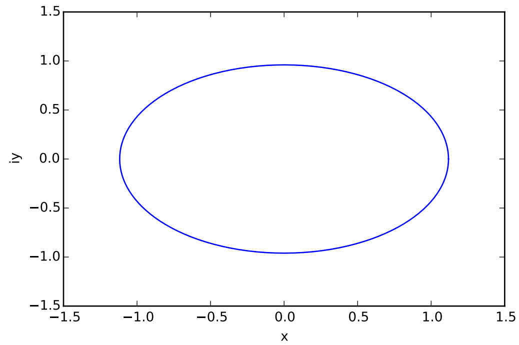

Figure 10. (Color online) ν contour for $c_1 = 1,\ c_0 = 0.5$.

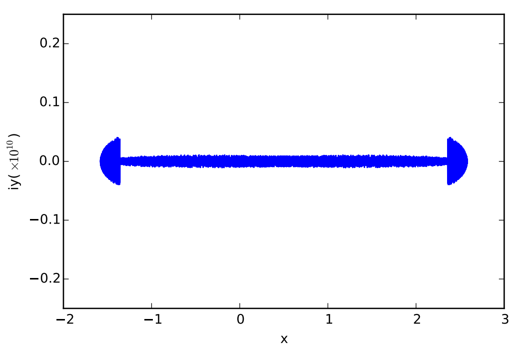

Figure 11. (Color online) Mapping for ν_1 contour, $c_1 = 1,\ c_0 = 0.5$. Mapping for ν_2 looks similar.

of locus of such points is given by

$$x^2 = \frac{1}{4} + \frac{y}{\tan(c_1 y)} - y^2. \tag{30}$$

Eq. (30) above forms a closed contour ν in complex plane which is symmetric about x-axis. We denote the two symmetric parts as curves ν_1 and ν_2 which are complex conjugates of each other. Figure 10 and Figure 11 show contour ν for $c_1 = 1, c_0 = 0.5$ and its mapping respectively.

Figure 12 shows schematically the mapping of all points on contour ν and all the regions in complex plane respectively by the JT $J_{c_1,c_0}(s)$. All points except the branch cut $[-\frac{1}{2}, \frac{1}{2}]$ inside region D bounded by contour ν are mapped to complex region $\mathbb{S}\backslash[a, b]$. All the points outside region D are mapped to a different complex region $\mathbb{C}\backslash[a, b]$.

We follow the method developed in Sections 3 and 4 to obtain an integral equation for the function $f(J_{c_1,c_0}(s))$. The g-functions of Eq. (8) are now replaced by

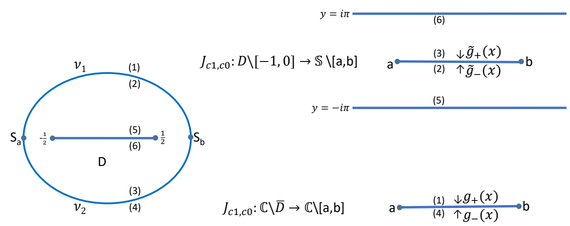

Figure 12. (Color online) Schematic Figure for mapping of JT, following CW.

$$
\begin{aligned}
g_e(z) &\equiv \int_a^b \log(z-x)d\mu(x), \qquad z \in \mathbb{C}\backslash(-\infty, b]; \\
\tilde{g}_e(z) &\equiv \int_a^b \log(e^z - e^x)d\mu(x), \quad z \in \mathbb{S}\backslash(-\infty, b].
\end{aligned}
\tag{31}
$$

Here $(g_e, \tilde{g}_e)$ are analytic in $(\mathbb{C}\backslash(-\infty, b), \mathbb{S}\backslash(-\infty, b))$ respectively so that the logarithms are well defined. Let g_{e+}, g_{e-} and $\tilde{g}_{e+}, \tilde{g}_{e-}$ denote boundary values of g_e and $\tilde{g}_e$ when approaching $[-\infty, b]$ respectively from above $(+)$ and below $(-)$. The M-functions of Eq. (12) are replaced by

$$
M_e(s) \equiv \begin{cases} G_e(J_{c_1,c_0}(s)), & \text{for } s \in \mathbb{C}\backslash\bar{D}, \\ \tilde{G}_e(J_{c_1,c_0}(s)), & \text{for } s \in D\backslash[-\frac{1}{2}, \frac{1}{2}], \end{cases} \tag{32}
$$

where as before, $G_e(s) \equiv g_e'(s)$ and $\tilde{G}_e(s) \equiv \tilde{g}_e'(s)$. The EL Eq. (13) remains the same, except that J is now a function of two parameters c_0 and c_1. The function $f_e(J_{c_1,c_0})(s)$ is now defined as

$$
f_e(J_{c_1,c_0})(s)) \equiv M_{e+}(s_1) + M_{e-}(s_1) = M_{e-}(s_2) + M_{e+}(s_2) \tag{33}
$$

with solution to $M_e(s)$ as,

$$
M_e(s) = \begin{cases} \frac{-1}{2\pi i} \oint_\nu \frac{f_e(J_{c_1,c_0})(\xi))}{\xi - s} d\xi, & s \in \mathbb{C}\backslash\bar{D}, \\ \frac{1}{2\pi i} \oint_\nu \frac{f_e(J_{c_1,c_0})(\xi))}{\xi - s} d\xi, & s \in D\backslash[-\frac{1}{2}, \frac{1}{2}]. \end{cases} \tag{34}
$$

As in Eq. (20) before, we define the inverse mapping,

$$
s_e = J^{-1}_{c_1,c_0}(x) = h_e(x). \tag{35}
$$

Note that for both $M_{e+}(s_1)$ and $M_{e-}(s_2)$ in Eq. (32), the function is the limit of $M(s)$ as $s \in \mathbb{C} \setminus \bar{D}$ approaches s_1 or s_2 on contour ν from outside. Hence we used first identity in Eq. (34). Let $(s_1)_{e+} = h_e(y)$; $(s_2)_{e-} = \bar{h}_e(y)$; $s_{1e} = h_e(x)$ and $s_{2e} = \bar{h}_e(x)$ where the bar denotes complex conjugate. In terms of the inverse mapping, the integral equation for f_e now has the form,

$$f_e(y;\gamma) = \frac{V'(y)}{\gamma} - \frac{1-\gamma}{\gamma 2\pi}\int_a^b f_e(x;\gamma)\phi_e(x,y)dx \tag{36}$$

where

$$\phi_e(x,y) = \mathrm{Im}\left[\left(\frac{1}{h_e(y)-\overline{h}_e(x)} + \frac{1}{\overline{h}_e(y)-\overline{h}_e(x)}\right)\overline{h}'_e(x)\right]. \tag{37}$$

As given in CW, the JT parameters c_1, c_0 satisfy the following equations,

$$\begin{gathered}\frac{1}{2\pi i}\oint_\nu U_{e;c_1,c_0}(s)ds = \frac{1}{c_1}, \quad \frac{1}{2\pi i}\oint_\nu \frac{U_{e;c_1,c_0}(s)}{s-\frac{1}{2}}ds = 1, \\ U_{c_1,c_0}(s) = f_e(J_{c_1,c_0}(s)).\end{gathered} \tag{38}$$

We solve the above integral equation (Eq. 36) for $f_e(y;\gamma)$ and Eq. (38) for c_1, c_0 numerically self-consistently. Using the definition for $f_e(x;\gamma)$ we further find the new effective potential $V_{\text{eff}}(x;\gamma)$ which is related to $f_e(x;\gamma)$ by

$$V'_{\text{eff}}(x;\gamma) = f_e(x;\gamma). \tag{39}$$

The corresponding density is computed using the formula from CW,

$$\sigma_e(y) = \frac{-1}{2\pi i}[M_{e+}(s_{e1}) - M_{e-}(s_{e2})]. \tag{40}$$

Substituting for $M_{e+}(s_{e1})$ and $M_{e-}(s_{e2})$, the expression for density becomes

$$\sigma_e(y;\gamma) = \frac{-1}{2\pi^2}\int_b^a f_e(x;\gamma)\chi_e(x,y)dx, \tag{41}$$

where

$$\chi_e(x,y) = \mathrm{Re}\left[\left(\frac{1}{\overline{h}_e(y)-h_e(x)} - \frac{1}{h_e(y)-h_e(x)}\right)h'_e(x)\right]. \tag{42}$$

References

[1] Mehta M L 2004 *Random matrices* 3rd ed (*Pure and Applied Mathematics (Amsterdam)* vol 142) (Elsevier/Academic Press, Amsterdam) ISBN 0-12-088409-7

[2] Beenakker C W J 1997 *Rev. Mod. Phys.* **69**(3) 731–808 URL `https://link.aps.org/doi/10.1103/RevModPhys.69.731`

[3] Muttalib K A 1995 *J. Phys. A* **28** L159–L164 ISSN 0305-4470 URL `http://stacks.iop.org/0305-4470/28/L159`

[4] Borodin A 1999 *Nuclear Phys. B* **536** 704–732 ISSN 0550-3213 URL `http://dx.doi.org/10.1016/S0550-3213(98)00642-7`

[5] Forrester P J and Wang D 2017 *Electron. J. Probab.* **22** Paper No. 54, 43 ISSN 1083-6489 URL `https://doi-org/10.1214/17-EJP62`

[6] Zhang L 2015 *J. Stat. Phys.* **161** 688–711 ISSN 0022-4715 URL `http://dx.doi.org/10.1007/s10955-015-1353-3`

[7] Kuijlaars A B J and Molag L D 2019 *Nonlinearity* **32** 3023–3081 URL https://doi.org/10.1088%2F1361-6544%2Fab247c

[8] Lueck T, Sommers H J and Zirnbauer M R 2006 *J. Math. Phys.* **47** 103304, 24 ISSN 0022-2488 URL http://dx.doi.org/10.1063/1.2356798

[9] Muttalib K A and Klauder J R 1999 *Phys. Rev. Lett.* **82**(21) 4272–4275 URL https://link.aps.org/doi/10.1103/PhysRevLett.82.4272

[10] Muttalib K A and Gopar V A 2002 *Phys. Rev. B* **66**(11) 115318 URL https://link.aps.org/doi/10.1103/PhysRevB.66.115318

[11] Douglas A, Markoš P and Muttalib K A 2014 *J. Phys. A* **47** 125103, 13 ISSN 1751-8113 URL https://doi-org/10.1088/1751-8113/47/12/125103

[12] Muttalib K A, Markoš P and Wölfle P 2005 *Phys. Rev. B* **72**(12) 125317 URL https://link.aps.org/doi/10.1103/PhysRevB.72.125317

[13] Muttalib K A, Pichard J L and Stone A D 1987 *Phys. Rev. Lett.* **59**(21) 2475–2478 URL https://link.aps.org/doi/10.1103/PhysRevLett.59.2475

[14] Deift P A 1999 *Orthogonal polynomials and random matrices: a Riemann-Hilbert approach* (*Courant Lecture Notes in Mathematics* vol 3) (New York: New York University Courant Institute of Mathematical Sciences) ISBN 0-9658703-2-4; 0-8218-2695-6

[15] Claeys T and Romano S 2014 *Nonlinearity* **27** 2419–2444 ISSN 0951-7715 URL http://dx.doi.org/10.1088/0951-7715/27/10/2419

[16] Claeys T and Wang D 2014 *Comm. Math. Phys.* **328** 1023–1077 ISSN 0010-3616 URL http://dx.doi.org/10.1007/s00220-014-1988-y